ADVANCED FUNCTIONAL MATERIALS
www.afm-journal.de

Epidermal Supercapacitor with High Performance

Pingshan Luan, Nan Zhang, Weiya Zhou, Zhiqiang Niu,* Qiang Zhang, Le Cai, Xiao Zhang, Feng Yang, Qingxia Fan, Wenbin Zhou, Zhuojian Xiao, Xiaogang Gu, Huiliang Chen, Kewei Li, Shiqi Xiao, Yanchun Wang, Huaping Liu, and Sishen Xie**

Recent development in epidermal and bionic electronics systems has promoted the increasing demand for supercapcacitors with micrometer-thickness and good compatibility. Here, a highly flexible free-standing epidermal supercapacitor (SC-E) with merely 1 µm thickness and high performance is developed. Single-walled carbon nanotube/poly(3,4-ethylenedioxythiophene) hybrid films with unique inner-connected reticulation are adopted as electrodes for ultrathin structure and high electric conductivity. Then, based on two substrates with different surface energies, a stepwise lift-off method is presented to peel off the ultrathin integrated supercapacitor from the substrates nondestructively. As a result of the high conductive hybrid electrodes and the thin electrolyte layer, the as-designed supercapacitors (based on the total mass of two electrodes) achieve a good capacitance of 56 F g^{-1} and a superhigh power density of 332 kW kg^{-1}, which manifest superior performance in contrast to the other devices fabricated by traditional electrodes. Meanwhile, the ultrashort response time of 11.5 ms enables the epidermal supercapacitor (SC-E) work for high-power units. More importantly, the free-standing structure and outstanding flexibility (10^5 times bending) endow the SC-E with excellent compatibility to be integrated and work in the next generation of smart and epidermal systems.

1. Introduction

The boom in portable consumer electronics has stimulated the development of epidermal components, which could be directly mounted onto the skin while integrating various functions, such as communication, health monitoring, and signal processing.[1–12] Recently, in order to serve on epidermis, many functional devices have been demonstrated with micrometer-thickness and outstanding compatibility.[1,5–8] As an indispensable unit of electronic system, energy storage devices are also required to design with extreme flexibility, sufficiently light weight, and especially ultrathin configuration, hence could match with epidermis[13] and other epidermal devices[1,5–8] (several microns for the thinnest thickness). Moreover, biomechanical energy conversion and miniaturized actuator have raised another emerging challenge for power-supply/storage units in their properties,

P. S. Luan,[+] Dr. N. Zhang, Prof. W. Y. Zhou, Q. Zhang, Dr. L. Cai,[++] Dr. X. Zhang, F. Yang, Q. X. Fan, Dr. W. B. Zhou, Z. J. Xiao, X. G. Gu, H. L. Chen, K. W. Li, S. Q. Xiao, Dr. Y. C. Wang, Prof. H. P. Liu, Prof. S. S. Xie
Beijing National Laboratory for Condensed Matter Physics
Institute of Physics
Chinese Academy of Sciences
Beijing 100190, China
E-mail: wyzhou@iphy.ac.cn; ssxie@iphy.ac.cn

P. S. Luan, Dr. N. Zhang, Prof. W. Y. Zhou, Q. Zhang, Dr. L. Cai, Dr. X. Zhang, F. Yang, Q. X. Fan, Dr. W. B. Zhou, Z. J. Xiao, X. G. Gu, H. L. Chen, K. W. Li, S. Q. Xiao, Dr. Y. C. Wang, Prof. H. P. Liu, Prof. S. S. Xie
Beijing Key Laboratory for Advanced Functional Materials and Structure Research
Beijing 100190, China

P. S. Luan, Dr. N. Zhang, Prof. W. Y. Zhou, Q. Zhang, Dr. L. Cai, Dr. X. Zhang, F. Yang, Q. X. Fan, Dr. W. B. Zhou, Z. J. Xiao, X. G. Gu, H. L. Chen, K. W. Li, S. Q. Xiao, Dr. Y. C. Wang, Prof. H. P. Liu, Prof. S. S. Xie
School of Physical Sciences
University of Chinese Academy of Sciences
Beijing 100049, China

Prof. Z. Q. Niu
Key Laboratory of Advanced Energy Materials Chemistry (Ministry of Education)
College of Chemistry
Collaborative Innovation Center of Chemical Science and Engineering
Nankai University
Tianjin 300071, China
E-mail: zqniu@nankai.edu.cn

[+]Present address: Department of Materials Science and Engineering, University of Maryland, College Park, MD 20742, USA
[++]Present address: Department of Electrical and Computer Engineering, Michigan State University, East Lansing, MI 48824, USA

DOI: 10.1002/adfm.201603480

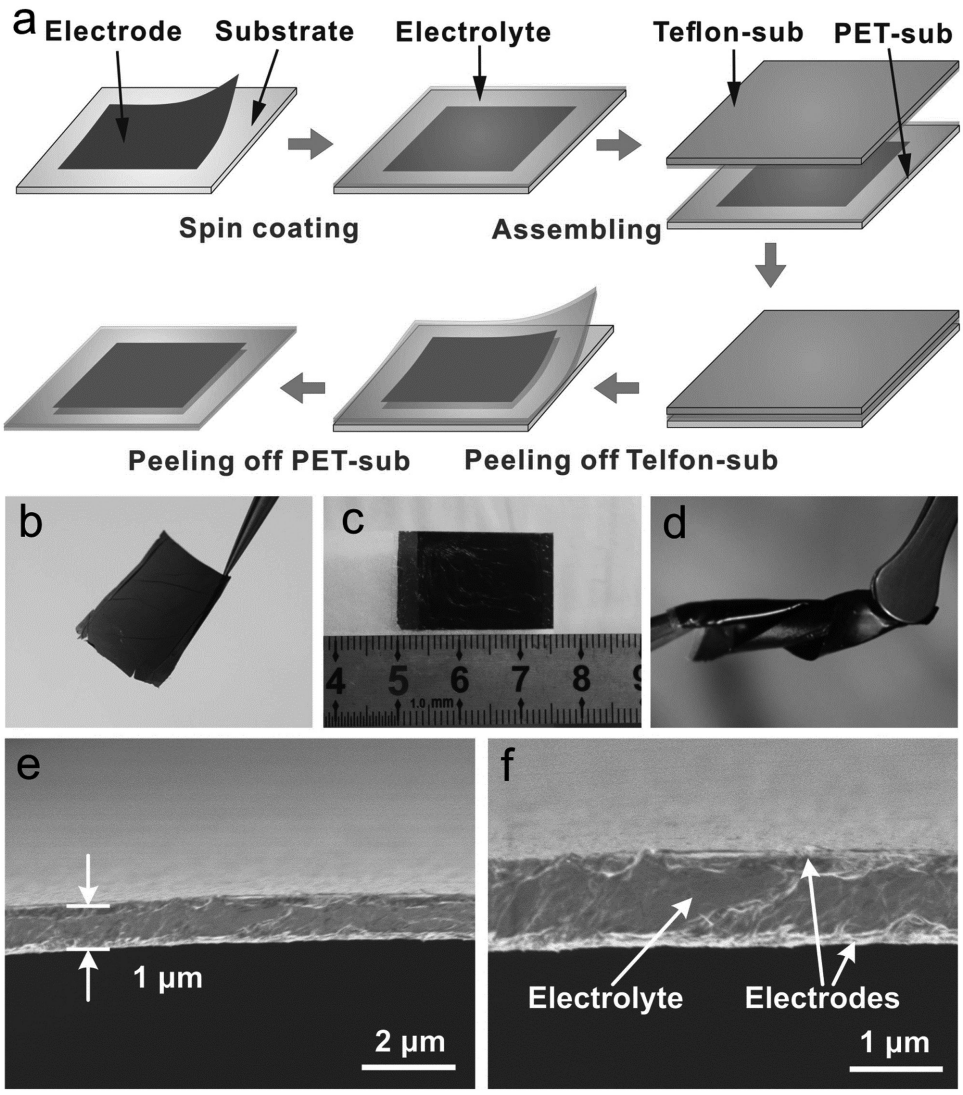

Figure 1. a) Schematic of assembling SC-E. Optical images of b) SWCNT/PEDOT hybrid film, c) as-prepared SC-E, and d) twisted SC-E. Cross-sectional SEM images of SC-E at e) low-magnification and f) high-magnification.

particularly in fast charge–discharge ability.[14–16] Nevertheless, the shortcoming in structure and performance of the existing energy storage devices has become the obstacle in building self-powered epidermal electronic system, thus limiting their applications. Supercapacitors, combining the advantage of capacitor and battery, have been regarded as an ideal candidate for future-generation power source in smart electronic products.[17–27] Based on graphene,[28–36] carbon nanotube,[37–48] and other nanoengineered electrodes,[49–54] some supercapacitors have achieved robust performance in capacitance and flexibility.

However, previous supercapacitors scaled down poorly in size.[55–61] Their integral thicknesses, typically larger than a hundred micrometer,[55,56] do not match with other components and impede the miniaturization of integrated devices.[1,5–7] Furthermore, due to the weak mechanical strength of the conventional electrodes and fabrication process, supercapacitors are generally substrate-dependent, which are not suitable as epidermal device and consequentially lead to extra weight.[56–61] Although some devices use ultrathin electrodes, they may suffer from inferior power performance as a result of the intrinsic high resistance of the materials. The incorporation of metal collectors, such as Au, could partly solve the issue but it would significantly restrict the flexibility and dramatically increase the cost.[56–60,62] Thus, seeking optimized electrode materials and developing novel assemble techniques are great challenges to construct a practical epidermal supercapacitor (SC-E) with high performance for a smart and self-powered system.

In this work, we have developed a highly flexible free-standing supercapacitor with 1 μm thickness and extraordinary power performance for epidermal electronic applications. An epidermal supercapacitor is designed and assembled as shown in **Figure 1**a. To overcome the disadvantages of traditional electrodes, a hybrid film (Figure 1b) of single-walled carbon nanotube/poly(3,4-ethylenedioxythiophene) (SWCNT/PEDOT) is adopted as a high conductive ultrathin electrode. Based on the substrates with different surface energies, we present a

stepwise lift-off technique to obtain the free-standing epidermal supercapacitor. The as-fabricated supercapacitor (Figure 1c–f), with the excellent flexibility (10^5 times bending) and ultrathin structure (≈1 μm), manifests the good compatibility and promising prospect for the next generation of epidermal electronics. In particular, their high power density and fast charge/discharge ability may expand the range of application in bionics and rapid energy storage.

2. Results and Discussion

To improve the capacitive performance of the electrode, PEDOT was deposited on the SWCNT film by cyclic voltammetry (CV) method. As shown in **Figure 2**a, when the CV cycle number is ten, the hybrid film offers an optimization between pore density and amount of PEDOT. Resulted from the double layer capacitance of reticulate structure and the pseudocapacitance of PEDOT, the specific capacitance of the electrode reaches maximum of 228 F g^{-1} with the PEDOT loading of about 70 wt%. The as-prepared hybrid film shows a high conductivity of about 1600 S cm^{-1} (Figure 2b), revealing remarkable improvement over conventional SWCNT hybrid electrodes.[22,63] The high conductivity of the electrode could reduce the ohmic resistance in the devices and enhance its power density accordingly. More importantly, the hybrid film could directly serve as both electrode and collector without metal materials. In addition, the breaking strain of the hybrid film decreases with the deposition cycle increasing (Figure 2c), because the PEDOT may restrict the deformation of SWCNT reticulation. The optimized hybrid film still possesses a good mechanical strength, and ensures that it could be easily handled and nondestructively separated from the substrate during the device assembly. However, the conventional ultrathin electrodes, limited by its mechanical properties, were generally unable to be peeled off from substrate.[56–61] Moreover, the electrode thickness-thinning process might increase its resistance, which would degrade the capacitive property and rate performance of the devices. Meanwhile, the combination of metal collector in electrode also increases the thickness and affects the flexibility.[56–60,62]

The scanning electron microscopy (SEM) images reveal the architecture feature of the as-prepared films. As shown in Figure 2d, the directly synthesized SWCNT film demonstrates a unique inner-connected reticulate structure with large amount of junctions in bundles (namely Y-shape junctions). Furthermore, the SWCNT bundles are also connected by Y-shape junctions after electrodeposition (Figure 2e). Therefore, in contrast to the overlap joint in the conventional electrodes,[55,64] the SWCNTs in the as-prepared film form a strong bonding and a continuous reticulation. For better understanding, the transmission electron microscopy (TEM) images of the Y-shape junction are presented in Figure 2f,g. Although the SWCNT bundles are uniformly wrapped by low conductive PEDOT (confirmed by Raman spectra and Fourier transform infrared (FTIR) spectra in Figure S3 in the Supporting Information), the conductive paths along SWCNT bundles are not destroyed. Hence, the inner-connected reticulation and the nanoporous network structure could provide ideal channels for charge transportation and electrolyte ion migration, respectively, which benefit the power characteristic of the supercapacitor. Besides, the inner-connected bundles also endow the inner-connected SWCNT/PEDOT reticulation with superior mechanical strength. Thus, the free-standing hybrid films with a thickness of only about 150 nm could be bent, folded, and even rolled-up to meet the

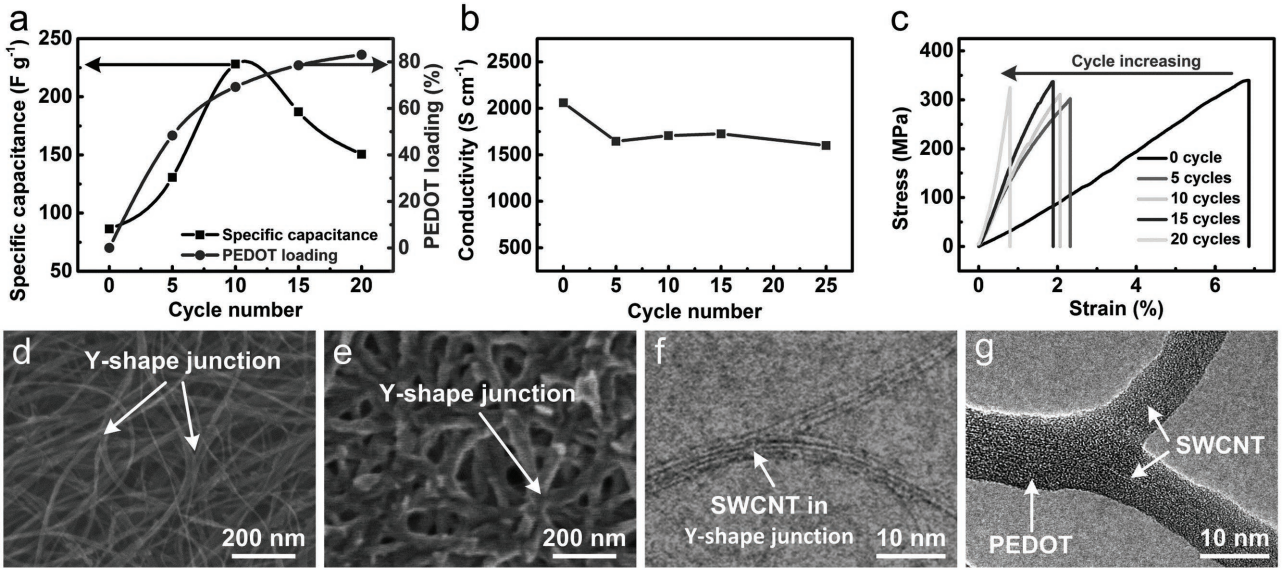

Figure 2. a) Specific capacitance and PEDOT loading (the mass ratio of the PEDOT) of the electrodes as a function of CV cycle number. The PEDOT loading was calculated by measuring the mass difference of the electrode before and after electrodeposition. b) Conductivity of the electrodes as a function of CV cycle number. c) Strain–stress curves of the electrodes at different electrodeposition cycles. SEM images of d) a pure SWCNT film and e) a hybrid film with ten cycles of electrodeposition. TEM images of f) a pure SWCNT film and g) a hybrid film with ten cycles of electrodeposition, in which SWCNT bundles are connected by Y-shape junctions.

requirement of both SC-E assembling process and further applications.

As reported in the previous work, free-standing supercapacitors are assembled usually by pressing the electrolyte-penetrating electrodes together or pasting the electrodes onto a solidified electrolyte membrane.[55,62] The thickness of electrolyte layer is difficult to control, particularly when it is reduced to a few microns. The electrolyte is hard to diffuse into the electrode thoroughly, leading to the device's performance degradation. In addition, the device, especially the electrode part, is prone to be damaged during the lift-off process. In this work, based on the SWCNT/PEDOT hybrid film, we adopt a spin coating method and develop a stepwise lift-off technique to fabricate SC-E. Two hybrid films are prespread on different substrates (Teflon-sub and polyethylene terephthalate (PET)-sub), then hot H_3PO_4-polyvinyl alcohol (PVA) gel electrolyte (85 °C) is cast and spin coated onto the films, as shown in Figure 1a. The thickness of the electrolyte layer could be adjusted by modulating spin speed and time. Then these two substrates, with electrodes and electrolyte, are pressed together and dried in room temperature. Due to the difference of substrate surface energies, the device could be peeled off from the substrate sequentially (first Teflon-sub then PET-sub). Finally, the free-standing supercapacitor with ultrathin configuration (about 1 μm in thickness) could be achieved, as shown in Figure 1c–f.

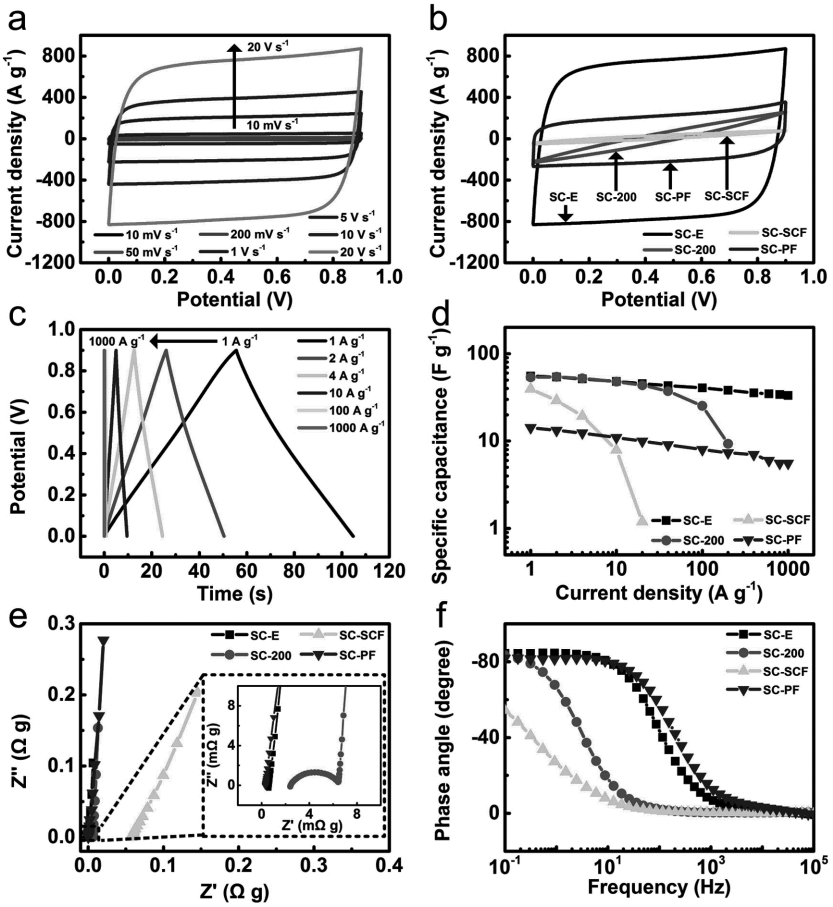

Figure 3. a) CVs of SC-E at different sweep rates. b) CVs of SC-E, SC-200, SC-SCF, and SC-PF at a sweep rate of 20 V s^{-1}. c) Galvanostatic charge and discharge curves of SC-E at different current densities. d) Specific capacitances of SC-E, SC-200, SC-SCF, and SC-PF at different current densities. e) Nyquist plots of SC-E, SC-200, SC-SCF, and SC-PF with a selected frequency from 100 mHz to 100 kHz. The impedances were normalized by the total mass of the hybrid electrodes for better comparison. Inset: enlargement of the part enclosed in the rectangle. f) Impedance phase angle as a function of frequency for SC-E, SC-200, SC-SCF, and SC-PF.

Figure 3a presents the cyclic voltammograms (CVs) of an as-prepared SC-E. With increasing scan rate, the SC-E manifests its outstanding high rate capability by a similar shape. The supercapacitor plots a rectangle CVs at a high scan rate of 20 V s^{-1}, which indicates the low resistance of the devices. Actually, the supercapacitor could work at a higher rate up to 100 V s^{-1} with a little distortion in CVs (Figure S4, Supporting Information). To better illustrate the rate performance of SC-E, we also fabricate the SWCNT/PEDOT supercapacitor with a thickness of about 200 μm (denoted as SC-200), the SWCNT/PEDOT supercapacitor based on solution-coated SWCNT film (denoted as SC-SCF, about 200 μm in thickness), and the ultrathin supercapacitor based on pure SWCNT film (denoted as SC-PF, about 1 μm in thickness). The details of fabricating process can be found in the Supporting Information. For comparison, the CVs of different supercapacitors at scan rate of 20 V s^{-1} are revealed in Figure 3b. The curves of SC-200 and SC-SCF are evidently distorted, which means the inferior high-rate performance resulted from the high equivalent series resistance (ESR) of the devices. However, the SC-E and SC-PF present a nearly rectangular CVs curve, indicating a rapid current response on voltage reversal and the low ESR of the whole device. Meanwhile, the area encircled by the CVs of SC-E is much larger than that of SC-PF, which represents a higher specific capacitance, since the PEDOT provides the faradaic pseudocapacitance effectively.

Figure 3c shows the galvanostatic charge and discharge curves of the supercapacitor, the SC-E works well even in wide current range from 1 to 1000 A g^{-1}. Calculated from the typical galvanostatic charge–discharge curves, the specific capacitances of the SC-E under different current densities are presented in Figure 3d. When the current density is 1 A g^{-1}, the specific capacitance of the SC-E reached about 56 F g^{-1} (the mass is the total mass of two hybrid electrodes), and the energy density is 6.0 W h kg^{-1}, which is comparable with previously reported PEDOT-based thick supercapacitors.[65,66] When the current density rises to 1000 A g^{-1}, the SC-E still operates well with a capacitance of 36 F g^{-1}. In contrast, specific capacitances of the SC-200 and SC-SCF fall off very quickly at ultrahigh charge/discharge rates. As shown in Figure 3d, because of the voltage drops in the test, the SC-200 and SC-SCF fail to charge and discharge at above 200 and 20 A g^{-1}, respectively.

The electrochemical impedance spectra (EIS) of the supercapacitors are shown as Nyquist plots in Figure 3e. The SC-E and SC-PF manifest a lower resistance compared to SC-200 and SC-SCF. The small ESR of the SC-E can be explained by the unique minimized pathway for ion diffusion and the superior conductivity of the electrode. According to the ESR and the mass of the both electrodes, the power density of the SC-E is 332 kW kg^{-1} in comparison with 31.6 kW kg^{-1} for SC-200, 3.5 kW kg^{-1} for SC-SCF, and 613 kW kg^{-1} for SC-PF. In Figure 3f, the response frequencies (f_{-45}, the frequency at the phase angle of –45°) of SC-E, SC-200, SC-SCF, and SC-PF are close to 87.0, 2.79, 0.23, and 184.2 Hz. The time constants ($1/f_{-45}$) of SC-E, SC-200, SC-SCF, and SC-PF are calculated as 11.5 ms, 358.4 ms, 4.3 s, and 5.4 ms, respectively. The SC-E achieves a higher power density and shorter response time compared to SC-200 and SC-SCF (SC-PF manifested a better performance in power density and response time because it is an electrical double layer capacitor and the conductivity of SWCNT film is higher than hybrid film, while the SC-PF suffers from the poor specific capacitance and energy density, as shown in Figure 3d). Furthermore, the power density of SC-E is higher than the ultrathin supercapacitor with metal collectors.[62] And the SC-E with short time constant (11.5 ms) shows ultrafast response compared to many previously reported values (10.7–19 ms) of the supercapacitors with metal collectors.[58,62] It is worth noting that the SC-E reported in this work is in the category of pseudocapacitor which generally has slower response. Additionally, comparing the supercapacitors with thicker electrodes (800 and 2000 nm), the SC-E with 150 nm thickness electrode manifested a better capacitive performance at high current density (Figure S5, Supporting Information), resulting from shorter migration distances for ion and electron.

The SC-E also exhibits great electrochemical stability during cyclic charging–discharging. As shown in Figure S6 (Supporting Information), the capacitance is mostly maintained during galvanostatic charge–discharge measurement for 1000 cycles. Furthermore, the SC-E can be stretched for 20% and bended without obvious changes in both CVs and EIS (Figure S7, Supporting Information), which implies its great potential in flexible electronic system. After bending for 10^5 times and stretching for 10^3 times, the capacitance of the device merely declined to about 90% and 95%, respectively. In addition, the leakage current of the SC-E rapidly drops to about 0.7 μA after 2 h (in Figure S8a, Supporting Information), which is lower than some commercial supercapacitors.[58,62] And in Figure S8b (Supporting Information), a stable open circuit voltage of about 0.6 V is well retained after 24 h, revealing a low self-discharge rate. Compared with the initial value, about 56% electric quantity of the supercapacitor is left. The performance of the supercapacitor is still stable after storage for 45 d (Figure S9, Supporting Information).

In **Figure 4**a, four SC-Es are easily used in series for a higher voltage and mounted on the demonstrator's fingers to power a red light-emitting diode (LED). The supercapacitors could illuminate a red LED whether the finger is straight or bent, confirming its potential for powering electronic devices. It should be noted that the supercapacitors were connected by SWCNT fibers (the schematic of the connection is shown in Figure S10 in the Supporting Information) rather than matel wires as shown in the enlarged images. More importantly, a SC-E, mounted on the demonstrator's wrist in Figure 4b–d, shows the texture of the skin. When the demonstrator strains the wrist upward or bends it, the SC-E is accordingly stretched or bent and even wrinkled with the skin, offering a better illustration of its ultrathin thickness and high flexibility.

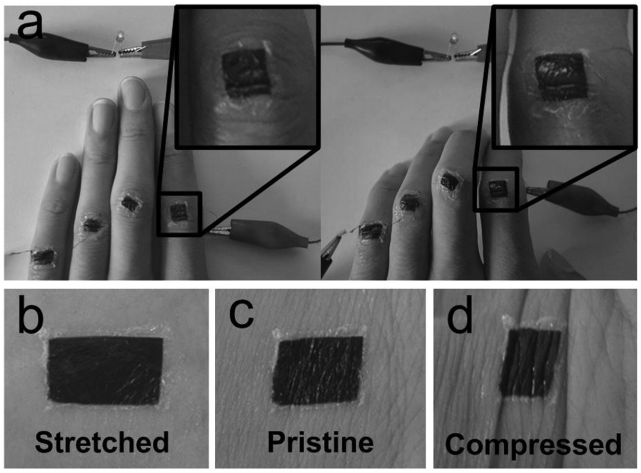

Figure 4. a) Optical image of four SC-Es in series mounted on the demonstrator's fingers powering a red LED when the finger was straight and bent. Inset: enlargement of the part enclosed in the rectangle. The electrodes of SC-E are connected with the CNT wires via a small piece of film, which could be easily pasted on the surface of the device. Optical images of SC-E mounted on demonstrator's wrist when the skin was b) stretched, c) pristine, and d) compressed. The supercapacitor was mounted on the skin by PVA or waterproof eyelash adhesive.

3. Conclusion

In summary, we have developed a free-standing integrated SC-E with excellent performance and a total of 1 micron thickness. Based on systematic research on the preparation of ultrathin SWCNT/PEDOT film and spin coating technique as well as stepwise lift-off method, the device's thickness is effectively controlled and the free-standing SC-E is achieved. Owing to the highly conductive hybrid electrode with an inner-connected reticulate structure and the ultrathin electrolyte layer, the integrated supercapacitor (based on the total mass of two electrodes) shows a superior specific capacitance of 56 F g^{-1} and superhigh power density of 332 kW kg^{-1} compared with the reported value for PEDOT-based supercapacitor. And the ultrashort response time of 11.5 ms enables the SC-E work for high-power units. More importantly, the SC-E with extreme flexibility (10^5 times bending) could be easily transferred and integrated onto epidermis without hindering the motion of the organism. Combined with its outstanding performance and good compatibility, the SC-E would exhibit great prospect for their application in fields of high-rate power sources and novel epidermal electronic devices. In addition, the highly efficient, highly repeatable, and easily scaling-up method demonstrated herein would be inspiring to develop other epidermal functional materials or devices with ultrathin and flexible feature.

4. Experimental Section

Preparation SWCNT/PEDOT Hybrid Film: Freestanding SWCNT film (100–200 nm in thickness) was prepared by the floating catalyst chemical vapor deposition method.[67] Subsequently, the SWCNT film was fixed on a frame and immersed in HNO_3 (15 mol L^{-1}) for 4 h to purify and functionalize with hydrophilic groups. Then, PEDOT was incorporated on the films to improve the capacitive performance of the electrodes. In a traditional three-electrode cell (saturated calomel electrode was used as reference electrode, platinum plate was used as counter electrode), PEDOT was electrodeposited into SWCNT films by CV at a potential cycle of 0–1 V with a scanning rate of 60 mV s^{-1}.[44] The electrolyte for electrodeposition was composed of 0.1 M toluene-4-sulfonic acid sodium salt and 0.01 M 3, 4-ethylenedioxythiophene in aqueous solution. After electrodeposition, the hybrid film could be peeled off from the frame. All chemicals were of analytical grade and all the electrochemical experiments were performed at room temperature.

Preparation of Solid Electrolyte Solution: PVA (3 g) and H_3PO_4 (3 g) were added into water (30 mL), and then the solution was heated and stirred at 85 °C for 2 h.

Assembly of Supercapacitor: The schematic of assembling supercapacitor was shown in Figure 1a. First, two kinds of substrate were prepared with different surface energy. Typically, polyethylene terephthalate (defined as PET-sub) and Teflon (defined as Teflon-sub) were selected as substrates. Two hybrid films were spread out onto the different substrates directly, and ethanol was dripped on the films to ensure flat. Then, the hot solid electrolyte solution (H_3PO_4-PVA aqueous solution, 85 °C) was dripped onto the hybrid films and coated the whole electrodes by a spin coater. The thickness of the electrolyte could be controlled by the spin rate and time. When the spin rate was 4000 r min^{-1} and coating time was 20 s, the ultrathin supercapacitor with a thickness of about 1 μm was successfully achieved. Faster spin rate and longer coating time would decrease the thickness, whereas the electrolyte might fail to separate the electrodes and result in the circuit short. After dried for 2 h, two substrates with hybrid electrodes and electrolyte gel were pressed together and dried for 48 h in the fume hood to accomplish assembling. Since the surface energy of Teflon was lower than that of PET, so the Teflon-sub possessed a weaker adhesive force with supercapacitor. During the separating process, the Teflon-sub with a lower adhesive force could be peeled off from the supercapacitor first. Then, the as-prepared supercapacitor was peeled off from PET-sub. It would be worth mentioning that some other materials with different surface energy, such as petri dish (polyethylene), silicon wafer, and glass slide, could also be used as the substrates.

Characterization and Measurement: The SEM images were obtained by Hitachi S-5200 and Hitachi S-4800, and TEM images by JEM-2010. The FTIR spectra were obtained by Varian Excalibur 3100. The Raman spectra were recorded by a microscopic confocal Raman spectrophotometer (HORIBA JY HR-800) with operating wavelength of 633 nm. The mechanical properties of the films were characterized by a dynamic mechanical analyzer (TA GG92-DMA Q800). The resistances of films were measured by Keithley-2400 sourcemeter. Electrodeposition and electrochemical tests were performed by electrochemical workstations (CHI 660C and Zahner IM6). The specific capacitance was calculated from the galvanostatic charge–discharge curves by using the equation $Cs = I/(m \times (V/t))$, where I was the applied current, t was the time of discharge, V was the window voltage, and m was the total mass of the electrodes. The mass was measured by a high precision balance (METTLER TOLEDO UMX2, the readability was 0.1 μg).

Supporting Information

Supporting Information is available from the Wiley Online Library or from the author.

Acknowledgements

P.S.L. and N.Z. contributed equally to this work. This work was supported by the National Basic Research Program of China (2012CB932302), the National Natural Science Foundation of China (51172271, 51372269, and 51472264), the "Strategic Priority Research Program" of the Chinese Academy of Sciences (XDA09040202), and the Beijing Municipal Education Commission (Grant No. YB20108000101). H.P.L. thanks support by the Recruitment Program of Global Youth Experts and the "100 talents project" of the CAS. Z.Q.N. thanks support by the NSFC (21573116), the Tianjin Basic and High-Tech Development (15JCYBJC17300).

Received: July 11, 2016
Revised: August 14, 2016
Published online: September 22, 2016

[1] D. H. Kim, N. S. Lu, R. Ma, Y. S. Kim, R. H. Kim, S. D. Wang, J. Wu, S. M. Won, H. Tao, A. Islam, K. J. Yu, T. I. Kim, R. Chowdhury, M. Ying, L. Z. Xu, M. Li, H. J. Chung, H. Keum, M. McCormick, P. Liu, Y. W. Zhang, F. G. Omenetto, Y. G. Huang, T. Coleman, J. A. Rogers, *Science* **2011**, *333*, 838.
[2] K. Nomura, H. Ohta, A. Takagi, T. Kamiya, M. Hirano, H. Hosono, *Nature* **2004**, *432*, 488.
[3] S. Xu, Y. Zhang, L. Jia, K. E. Mathewson, K.-I. Jang, J. Kim, H. Fu, X. Huang, P. Chava, R. Wang, S. Bhole, L. Wang, Y. J. Na, Y. Guan, M. Flavin, Z. Han, Y. Huang, J. A. Rogers, *Science* **2014**, *344*, 70.
[4] R. C. Webb, A. P. Bonifas, A. Behnaz, Y. Zhang, K. J. Yu, H. Cheng, M. Shi, Z. Bian, Z. Liu, Y. S. Kim, W. H. Yeo, J. S. Park, J. Song, Y. Li, Y. Huang, A. M. Gorbach, J. A. Rogers, *Nat. Mater.* **2013**, *12*, 938.
[5] M. Kaltenbrunner, T. Sekitani, J. Reeder, T. Yokota, K. Kuribara, T. Tokuhara, M. Drack, R. Schwodiauer, I. Graz, S. Bauer-Gogonea, S. Bauer, T. Someya, *Nature* **2013**, *499*, 458.
[6] W. H. Yeo, Y. S. Kim, J. Lee, A. Ameen, L. Shi, M. Li, S. Wang, R. Ma, S. H. Jin, Z. Kang, Y. Huang, J. A. Rogers, *Adv. Mater.* **2013**, *25*, 2773.
[7] A. Chortos, Z. Bao, *Mater. Today* **2014**, *17*, 321.
[8] X. Huang, Y. Liu, H. Cheng, W.-J. Shin, J. A. Fan, Z. Liu, C.-J. Lu, G.-W. Kong, K. Chen, D. Patnaik, S.-H. Lee, S. Hage-Ali, Y. Huang, J. A. Rogers, *Adv. Funct. Mater.* **2014**, *24*, 3845.
[9] B. Xu, A. Akhtar, Y. Liu, H. Chen, W.-H. Yeo, S. ParkII, B. Boyce, H. Kim, J. Yu, H.-Y. Lai, S. Jung, Y. Zhou, J. Kim, S. Cho, Y. Huang, T. Bretl, J. A. Rogers, *Adv. Mater.* **2016**, *28*, 4462.
[10] J. Kim, A. Banks, H. Cheng, Z. Xie, S. Xu, K.-I. Jang, J. W. Lee, Z. Liu, P. Gutruf, X. Huang, P. Wei, F. Liu, K. Li, M. Dalal, R. Ghaffari, X. Feng, Y. Huang, S. Gupta, U. Paik, J. A. Rogers, *Small* **2015**, *11*, 906.
[11] Y. Zhai, L. Mathew, R. Rao, D. Xu, S. K. Banerjee, *Nano Lett.* **2012**, *12*, 5609.
[12] A. Chortos, G. I. Koleilat, R. Pfattner, D. Kong, P. Lin, R. Nur, T. Lei, H. Wang, N. Liu, Y.-C. Lai, M.-G. Kim, J. W. Chung, S. Lee, Z. Bao, *Adv. Mater.* **2016**, *28*, 4441.
[13] J. T. Whitton, J. Everall, *Br. J. Dermatol.* **1973**, *89*, 467.
[14] T. I. Lee, S. Lee, E. Lee, S. Sohn, Y. Lee, S. Lee, G. Moon, D. Kim, Y. S. Kim, J. M. Myoung, Z. L. Wang, *Adv. Mater.* **2013**, *25*, 2920.
[15] S. Taccola, F. Greco, E. Sinibaldi, A. Mondini, B. Mazzolai, V. Mattoli, *Adv. Mater.* **2015**, *27*, 1668.
[16] S. Y. Chung, S. Kim, J.-H. Lee, K. Kim, S.-W. Kim, C.-Y. Kang, S.-J. Yoon, Y. S. Kim, *Adv. Mater.* **2012**, *24*, 6022.
[17] M. Beidaghi, Y. Gogotsi, *Energy Environ. Sci.* **2014**, *7*, 867.
[18] L. Hu, Y. Cui, *Energy Environ. Sci.* **2012**, *5*, 6423.
[19] X. Wang, X. Lu, B. Liu, D. Chen, Y. Tong, G. Shen, *Adv. Mater.* **2014**, *26*, 4763.

[20] Z. Niu, L. Liu, L. Zhang, W. Zhou, X. Chen, S. Xie, *Adv. Energy Mater.* **2015**, *5*, 1500677.
[21] X. Cao, C. Tan, X. Zhang, W. Zhao, H. Zhang, *Adv. Mater.* **2016**, *28*, 6167.
[22] L. B. Hu, M. Pasta, F. La Mantia, L. F. Cui, S. Jeong, H. D. Deshazer, J. W. Choi, S. M. Han, Y. Cui, *Nano Lett.* **2010**, *10*, 708.
[23] U. N. Maiti, J. Lim, K. E. Lee, W. J. Lee, S. O. Kim, *Adv. Mater.* **2014**, *26*, 615.
[24] Z. Niu, W. Zhou, J. Chen, G. Feng, H. Li, W. Ma, J. Li, H. Dong, Y. Ren, D. Zhao, *Energy Environ. Sci.* **2011**, *4*, 1440.
[25] S. Z. Wang, L. Zhang, C. L. Sun, Y. L. Shao, Y. Z. Wu, J. X. Lv, X. P. Hao, *Adv. Mater.* **2016**, *28*, 3768.
[26] C. Xu, Z. H. Li, C. Yang, P. C. Zou, B. H. Xie, Z. Y. Lin, Z. X. Zhang, B. H. Li, F. Y. Kang, C. P. Wong, *Adv. Mater.* **2016**, *28*, 4105.
[27] K. Yuan, Y. Z. Xu, J. Uihlein, G. Brunklaus, L. Shi, R. Heiderhoff, M. M. Que, M. Forster, T. Chasse, T. Pichler, T. Riedl, Y. W. Chen, U. Scherf, *Adv. Mater.* **2015**, *27*, 6714.
[28] L. Liu, Z. Niu, L. Zhang, W. Zhou, X. Chen, S. Xie, *Adv. Mater.* **2014**, *26*, 4855.
[29] G. X. Qu, J. L. Cheng, X. D. Li, D. M. Yuan, P. N. Chen, X. L. Chen, B. Wang, H. S. Peng, *Adv. Mater.* **2016**, *28*, 3646.
[30] J. Xie, X. Sun, N. Zhang, K. Xu, M. Zhou, Y. Xie, *Nano Energy* **2013**, *2*, 65.
[31] Z. Xiong, C. Liao, W. Han, X. Wang, *Adv. Mater.* **2015**, *27*, 4469.
[32] Y. Liu, B. Weng, J. M. Razal, Q. Xu, C. Zhao, Y. Hou, S. Seyedin, R. Jalili, G. G. Wallace, J. Chen, *Sci. Rep.* **2015**, *5*, 17045.
[33] Z. Q. Niu, J. Chen, H. H. Hng, J. Ma, X. D. Chen, *Adv. Mater.* **2012**, *24*, 4144.
[34] Y. Hu, C. Guan, G. Feng, Q. Ke, X. Huang, J. Wang, *Adv. Funct. Mater.* **2015**, *25*, 7291.
[35] Z. Ling, Z. Wang, M. Zhang, C. Yu, G. Wang, Y. Dong, S. Liu, Y. Wang, J. Qiu, *Adv. Funct. Mater.* **2016**, *26*, 111.
[36] D. T. Pham, T. H. Lee, D. H. Luong, F. Yao, A. Ghosh, V. T. Le, T. H. Kim, B. Li, J. Chang, Y. H. Lee, *ACS Nano* **2015**, *9*, 2018.
[37] Z. Niu, P. Luan, Q. Shao, H. Dong, J. Li, J. Chen, D. Zhao, L. Cai, W. Zhou, X. Chen, *Energy Environ. Sci.* **2012**, *5*, 8726.
[38] J. A. Lee, M. K. Shin, S. H. Kim, S. J. Kim, G. M. Spinks, G. G. Wallace, R. Ovalle-Robles, M. D. Lima, M. E. Kozlov, R. H. Baughman, *ACS Nano* **2012**, *6*, 327.
[39] Z. Q. Niu, H. B. Dong, B. W. Zhu, J. Z. Li, H. H. Hng, W. Y. Zhou, X. D. Chen, S. S. Xie, *Adv. Mater.* **2013**, *25*, 1058.
[40] G. Sun, X. Zhang, R. Lin, B. Chen, L. Zheng, X. Huang, L. Huang, W. Huang, H. Zhang, P. Chen, *Adv. Electron. Mater.* **2016**, *2*, 1600102.
[41] N. Zhang, P. Luan, W. Zhou, Q. Zhang, L. Cai, X. Zhang, W. Zhou, Q. Fan, F. Yang, D. Zhao, Y. Wang, S. Xie, *Nano Res.* **2014**, *7*, 1680.
[42] Z. Zhang, J. Deng, X. Li, Z. Yang, S. He, X. Chen, G. Guan, J. Ren, H. Peng, *Adv. Mater.* **2015**, *27*, 356.
[43] Z. Q. Niu, W. Y. Zhou, X. D. Chen, J. Chen, S. S. Xie, *Adv. Mater.* **2015**, *27*, 6002.
[44] N. Zhang, W. Zhou, Q. Zhang, P. Luan, L. Cai, F. Yang, X. Zhang, Q. Fan, W. Zhou, Z. Xiao, X. Gu, H. Chen, K. Li, S. Xiao, Y. Wang, H. Liu, S. Xie, *Nanoscale* **2015**, *7*, 12492.
[45] J. Ren, W. Y. Bai, G. Z. Guan, Y. Zhang, H. S. Peng, *Adv. Mater.* **2013**, *25*, 5965.
[46] J. Ren, L. Li, C. Chen, X. L. Chen, Z. B. Cai, L. B. Qiu, Y. G. Wang, X. R. Zhu, H. S. Peng, *Adv. Mater.* **2013**, *25*, 1155.
[47] X. Chen, H. Lin, P. Chen, G. Guan, J. Deng, H. Peng, *Adv. Mater.* **2014**, *26*, 4444.
[48] H. Sun, X. Fu, S. Xie, Y. Jiang, G. Guan, B. Wang, H. Li, H. Peng, *Adv. Mater.* **2016**, *28*, 6429.
[49] R. Vellacheri, H. Zhao, M. Mühlstädt, J. Ming, A. Al-Haddad, M. Wu, K. D. Jandt, Y. Lei, *Adv. Mater. Technol.* **2016**, *1*, 1600012.
[50] X. Yu, X. Su, K. Yan, H. Hu, M. Peng, X. Cai, D. Zou, *Adv. Mater. Technol.* **2016**, *1*, 1600009.
[51] H. Y. Jung, M. B. Karimi, M. G. Hahm, P. M. Ajayan, Y. J. Jung, *Sci. Rep.* **2012**, *2*, 773.
[52] Y. Song, T.-Y. Liu, X.-X. Xu, D.-Y. Feng, Y. Li, X.-X. Liu, *Adv. Funct. Mater.* **2015**, *25*, 4626.
[53] G. Zhang, Y. Song, H. Zhang, J. Xu, H. Duan, J. Liu, *Adv. Funct. Mater.* **2016**, *26*, 3012.
[54] Y. B. Yin, J. J. Xu, Q. C. Liu, X. B. Zhang, *Adv. Mater.* **2016**, *28*, 7494.
[55] C. Z. Meng, C. H. Liu, L. Z. Chen, C. H. Hu, S. S. Fan, *Nano Lett.* **2010**, *10*, 4025.
[56] Z. Niu, L. Zhang, L. Liu, B. Zhu, H. Dong, X. Chen, *Adv. Mater.* **2013**, *25*, 4035.
[57] J. J. Yoo, K. Balakrishnan, J. Huang, V. Meunier, B. G. Sumpter, A. Srivastava, M. Conway, A. L. Mohana Reddy, J. Yu, R. Vajtai, P. M. Ajayan, *Nano Lett.* **2011**, *11*, 1423.
[58] M. F. El-Kady, R. B. Kaner, *Nat. Commun.* **2013**, *4*, 1475.
[59] J. Feng, X. Sun, C. Wu, L. Peng, C. Lin, S. Hu, J. Yang, Y. Xie, *J. Am. Chem. Soc.* **2011**, *133*, 17832.
[60] C. Wu, X. Lu, L. Peng, K. Xu, X. Peng, J. Huang, G. Yu, Y. Xie, *Nat. Commun.* **2013**, *4*, 2431.
[61] M. Kaempgen, C. K. Chan, J. Ma, Y. Cui, G. Gruner, *Nano Lett.* **2009**, *9*, 1872.
[62] F. Meng, Y. Ding, *Adv. Mater.* **2011**, *23*, 4098.
[63] J.-E. Huang, X.-H. Li, J.-C. Xu, H.-L. Li, *Carbon* **2003**, *41*, 2731.
[64] L. Hu, D. S. Hecht, G. Grüner, *Nano Lett.* **2004**, *4*, 2513.
[65] B. Anothumakkool, R. Soni, S. N. Bhange, S. Kurungot, *Energy Environ. Sci.* **2015**, *8*, 1339.
[66] D. Antiohos, G. Folkes, P. Sherrell, S. Ashraf, G. G. Wallace, P. Aitchison, A. T. Harris, J. Chen, A. I. Minett, *J. Mater. Chem.* **2011**, *21*, 15987.
[67] W. J. Ma, L. Song, R. Yang, T. H. Zhang, Y. C. Zhao, L. F. Sun, Y. Ren, D. F. Liu, L. F. Liu, J. Shen, Z. X. Zhang, Y. J. Xiang, W. Y. Zhou, S. S. Xie, *Nano Lett.* **2007**, *7*, 2307.